scientific reports

Check for updates

OPEN

Dynamic mechanical behavior and energy dissipation characteristics of low-temperature saturated granite under cyclic impact loading

Huaqiao Xu[1], Chuanxin Rong[1]✉, Bin Wang[1], Qinghe Zhang[1], Zhijun Shen[2] & Yi Jin[2]

To investigate the dynamic mechanical behavior and energy dissipation characteristics of low-temperature rock samples under cyclic impact loading, a temperature-controlled impact system that combines Hopkins bars with a low-temperature compensation device was used. Five temperature gradients were confirmed via a trial impact test, and impact tests were conducted under two kinds of impact air pressures. The macroscopic damage characteristics of rock samples under cyclic impact at different temperatures, dynamic stress-strain curves, changes in peak stress and strain, energy dissipation, and cumulative damage at different temperatures, and the macroscopic and microscopic structural characteristics of low-temperature rock samples after cyclic impact were analyzed in combination with damage. The findings indicated that low-temperature saturated granite primarily experienced tensile damage under cyclic impact loading, with the required number of impacts increasing with decreasing temperature, and rock samples exhibited freeze-induced brittleness and significantly increased fragmentation. The dynamic stress-strain curve generally exhibited rebound characteristics in the post-peak stage. With an increasing number of cycles, an overall decrease in peak stress was observed, whereas the peak strain and cumulative specific dissipated energy exhibited opposite trends. This trend was more pronounced at lower temperatures, with a significant increase in peak strain and specific energy amplitude. In addition, the cumulative damage factor of the rock samples increased at lower temperatures, consistent with macroscopic damage characteristics, and exhibited a negative correlation with peak stress. The degree of crack extension in the macroscopic samples corresponded with the observed fracture changes. Microanalysis (SEM) indicated that decreasing temperature resulted in freeze brittleness of the fracture surfaces, characterized by reduced flatness and an expansion of brittle cracks across the damage surface. The slip separation phenomenon became increasingly pronounced, and these observations were positively correlated with the cumulative damage value.

Keywords Saturated granite, Cyclic impact, Dynamic mechanical behavior, Energy dissipation, Low-temperature compensation

There has been a rapid increase in the construction of large-scale geotechnical structures as China's economy continues to expand. This has introduced numerous challenges in the field of rock construction. Drilling and blasting of underground chambers and blasting of palm faces continue to be the most significant construction methods[1]. During tunnel construction, the rocks surrounding the tunnel are subjected to cyclic and repeated dynamic loads, leading to cumulative rock damage. When this damage reaches the collapse threshold, it can result in a collapse, with the induced rock instability posing a serious threat to the safety of the project[2–4]. In addition, several climatic and geological conditions lead to numerous challenges. Therefore, a comprehensive investigation of the mechanical response and energy evolution of rocks under cyclic impact loading at diverse temperatures is critical for engineering.

To date, numerous scholars have focused on the dynamic mechanics of rock-like materials under cyclic loading, particularly at low temperatures. Jin[5] employed a self-designed SHPB apparatus and investigated the typical dynamic stress-strain curve of rock during cyclic impact loading. He analyzed the reflected and transmitted

[1]School of Civil Engineering and Architecture, Anhui University of Science and Technology, 232001 Huainan, Anhui Province, China. [2]China Railway No.4 Engineering Group Co, Ltd, 230023 Hefei, Anhui, China. ✉email: chxrong@aust.edu.cn

wave patterns and delineated the stress-strain curve into five distinct stages. Li[6] performed uniaxial cyclic impact tests on granite and revealed that the rock exhibited a significant damage threshold at dynamic loads below a certain value. In another study, Wang[7] employed an optimized separated Hopkins rod for uniform amplitude cyclic impact on granite. The resulting static crack initiation stress, obtained from the static compressive stress-strain curve, was enhanced by the strength growth scaling factor to derive the dynamic crack initiation stress, thus elucidating the experimentally observed phenomena. Shu[8] also utilized a modified detached Hopkins bar to study the influence law of heat-treated rocks under cyclic impact and reported that the dissipation capacity and fracture strength of rocks decreased with increasing temperature and that the rocks more easily fractured. Ping[9] conducted impact compression tests under annular confinement and revealed that rock samples exhibited enhanced performance when subjected to passive confinement. Compared with the unconfined condition, the axial stress experienced by the sample increased by 20%, whereas the destructive strain increased by 2–3 times. This threshold was approximately 60% of the uniaxial compressive strength of the rock. Cao[10] employed cyclic impact and type II fracture toughness experiments to examine the damage and fracture characteristics of marble samples under different dynamic damage levels. He analyzed how different properties of marble deteriorate after impact damage and assessed the damage level from an energy perspective using acoustic emission technology. The energy dissipation and mechanical properties of rocks under dynamic cyclic impact have been thoroughly studied by the above scholars. However, in actual engineering, rocks are affected not only by multiple impact loads but also by changes in rock temperature as well as heat treatment and cooling during external mining[11–13]. Therefore, when studying the effects of cyclic impact loading, changes in environmental conditions must be comprehensively considered.

In deep rock engineering, temperature is an important factor that affects the mechanical properties of rocks[14–16], and many scholars have addressed the factor of temperature. Huang[17] conducted comparative tensile and uniaxial compressive strength tests on marble, sandstone, and granite samples under varying water content states (dry vs. saturated) before and after freezing with liquid nitrogen. However, blasting and excavation structures in alpine regions require an understanding of rock dynamics under low-temperature conditions. Wang[18] investigated the effect of temperature on saturated granite at high strain rates. He reported that the relationships of peak strain and damage variables with temperature indicate the effect of temperature on the strength of saturated granite after freezing, with low temperatures potentially increasing its strength. Zhang[19] designed tests under the composite effect of freeze-thaw cycles and cyclic impact to study the mechanical behavior of red sandstone. Meng[20] analyzed the variation rule of the microstructure of red sandstone with the number of freeze-thaw cycles and reported that the internal structure of red sandstone exhibited an osmotic expansion phenomenon and that with an increasing number of cycles, this phenomenon became more obvious. Shu et al.[21] conducted cyclic impact experiments on granite following treatments at different high temperatures, simulating high geothermal environment conditions within a deep rock body. Wang et al.[22,23] investigated the dynamic properties and energy evolution of granite under cyclic dynamic loading when subjected to different heat treatment conditions using the SHPB test setup. The results revealed a rapid deterioration in the mechanical properties of the rock at 600 °C, whereas at 200 °C, the number of microfractures within the granite samples decreased, indicating a significant temperature effect. It is evident that temperature-related dynamic mechanical tests are performed mainly by pretreating rock samples beforehand, and less research has been done on this aspect of dynamic mechanical tests without considering the real-time temperature environment. The rock samples subjected to temperature-related dynamic mechanical tests, mainly high- and low-temperature treatments or freeze–thaw treatment, are pretreated without considering the real-time temperature conditions for dynamic mechanical tests; this aspect of the study is limited.

Briefly, scientists have performed in-depth studies on rock mechanical properties, energy dissipation, and damage modes while investigating dynamic mechanical problems under cyclic loading and in real-time cryogenic environments. However, only a few experimental studies have combined these two aspects to analyze rock characteristics comprehensively. In this context, this study combined the aspects of cyclic loading action and low-temperature conditions to investigate the dynamic mechanical properties and damage morphology of low-temperature saturated granite under cyclic impact loading using SHPB dynamic impact tests in combination with a low-temperature compensation system. This study focused on the principles of energy loss and damage changes, integrating an experimental method to reveal the evolution of damage to low-temperature saturated granite under the action of cyclic impact loading. This study provides a significant reference value for engineering planning, design, and construction for studying the mechanical properties of low-temperature saturated granite under dynamic loading.

Preparation and testing of cryogenic samples

Specimen preparation

The test material was collected from the rock surrounding the tunnel at a site of the CZ Railway. The rock samples were grayish white, with their major components comprising mcroplagioclase feldspar (41%), plagioclase feldspar (28%), quartz (23%), and other minerals such as black mica (7%). For the SHPB cyclic test, an L/D ratio of the brittle rock material between 0.4 and 0.5 was chosen to obtain a complete stress-strain curve[7,24]. Therefore, the L/D ratio of the sample in this test was 0.467, and the granite sample was processed into a short cylindrical shape of 75 mm × 35 mm. To ensure experimental accuracy and reduce the influence of differences in the physical properties of rock on the experimental results, granite samples with uniform layering and no evident crack defects were chosen for the experiments. Moreover, ultrasonic testing of the rock samples was performed to remove samples with large wave velocity dispersion, as was nuclear magnetic resonance (NMR) testing of the distribution pattern of the T_2 spectrum of the rock samples and stripping of samples with large pore size dispersion, as shown in (Fig. 1). Table 1 presents the basic physical and mechanical parameters of the granite samples.

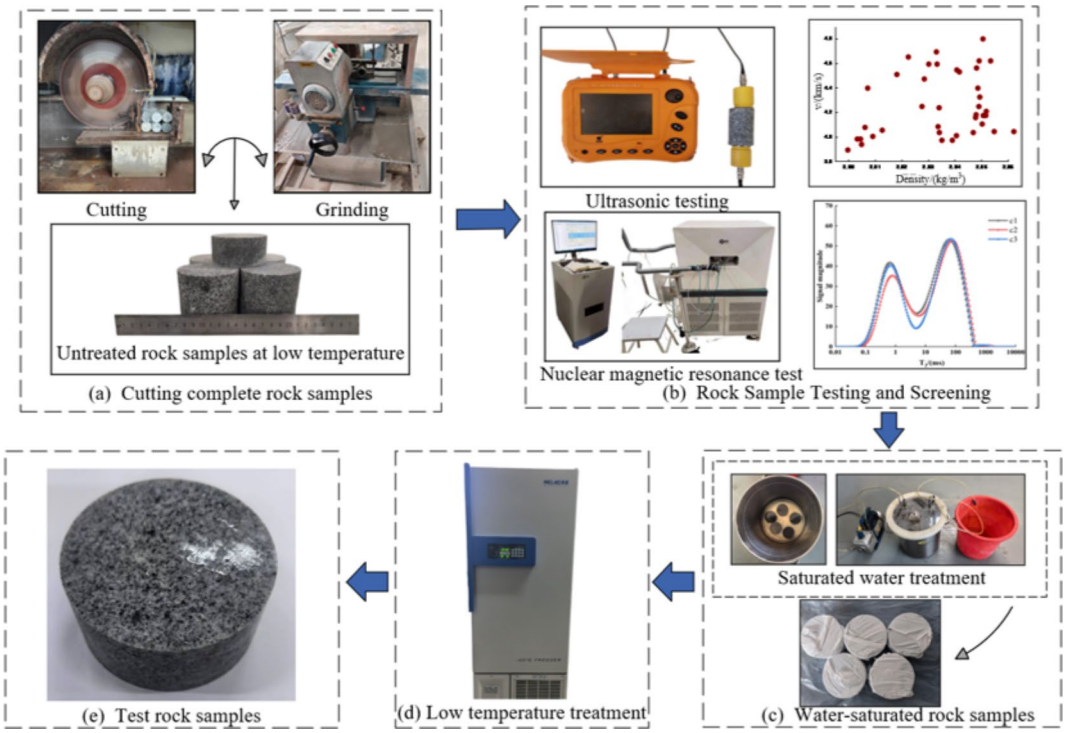

Fig. 1. Preparation process of rock sample.

Dry density/(kg/m^{-3})	Saturated density/(kg/m^{-3})	Strength of compress/MPa	Tension strength/MPa	Longitudinal wave velocity/(m/s)
2838	2857	140.86	6.68	4405

Table 1. Basic physical and mechanical parameters of the granite samples.

The test employed a method of coupling low-temperature loading and cyclic impact loading to examine the dynamic mechanical properties of the rock. Before testing, the cut and polished rock samples were saturated with water, followed by different cooling treatments applied to their two separate parts: (1) one part of the sample, which was free of obvious defects in the stratification of the granite sample, was chosen and placed into a vacuum water bath box and left static for 24 h; (2) the other part of the sample was saturated following uniform coating with Vaseline and wrapped in waterproof tape wrapped before being placed in the high- and low-temperature testing machine for cooling treatment. After the samples were cooled to the predetermined temperature and stabilized for 24 h in the high and low-temperature testing machine, they were quickly transferred to the SHPB testing system to complete dynamic mechanical property testing of the low-temperature rock samples. The specific test rock sample preparation process is shown in (Fig. 1).

Testing equipment

As shown in Fig. 2, the test is conducted with the improved SHPB test system. The test system primarily comprises a gas storage chamber, bullet velocity infrared detection system, impact warhead, compression rod (impact rod, transmission rod, and buffer rod), acquisition system (dynamic strain gauge and data acquisition system), and compression rod for high-strength alloy steel. The system exhibited a longitudinal wave velocity of 5172 m/s, a Young's modulus of 210 GPa, and impact and transmission rod lengths of 2400 mm and 1200 mm, respectively. Considering that the temperature of a sample during the cyclic impact process gradually decreases with time, a cryogenic device was employed to mitigate the impact of room temperature fluctuations. As shown in Fig. 2, a cryogenic compensation system (cryogenic nitrogen, a temperature console, and a cryogenic compensation sealing box) is installed between the incidence rod and transmission rod. For the purposes and requirements of the test, the temperature of the environment in the cryogenic confinement chamber is monitored in real time using a temperature control table, and the flow rate of supplied cryogenic nitrogen is adjusted to compensate for temperature loss in the test environment and during the operating process to ensure that the temperature in the confinement chamber is consistent with that of the cryogenically treated rock samples in the initial state and during the test process. This process helps minimize test errors and ensures the accuracy and reliability of the test results. Moreover, to eliminate waveform oscillations during the loading process, a thin circular rubber spacer is glued to the front center of the incident rod for filtering.

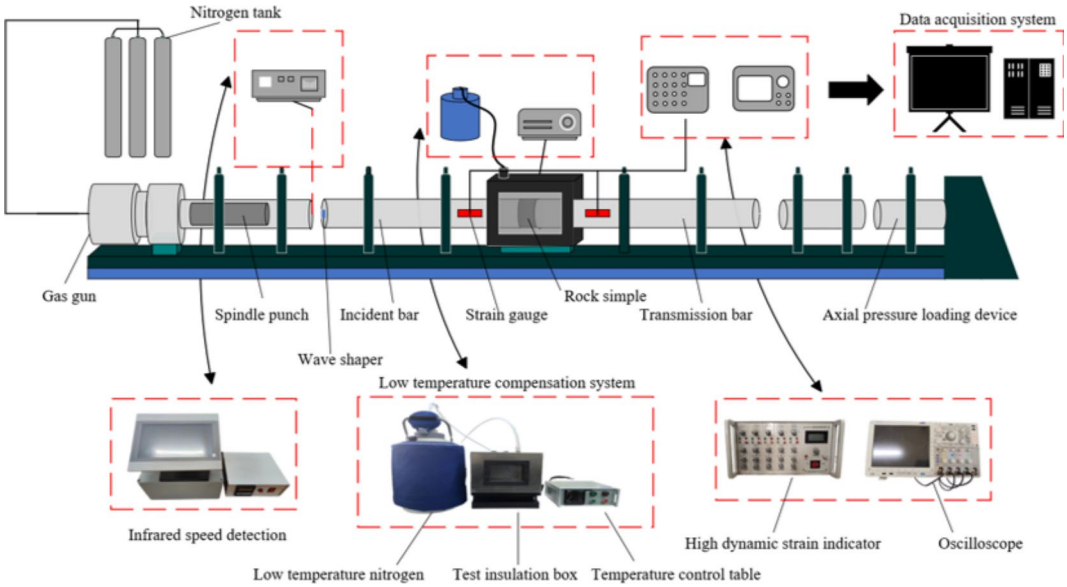

Fig. 2. Hopkinson pressure bar test system.

Experimental scheme

To avoid one-time impact damage to the sample and ensure that cyclic loading can be performed, pre-impact tests are necessary to determine the appropriate impact load. First, the bullet position within the firing cavity was fixed, and then the impact air pressure on the sample test die was adjusted. Finally, the impact air pressure of this batch of granite samples was within 0.3–0.6 MPa (strain rate of 26–55 s^{-1}), effectively achieving cyclic impact. Therefore, for this experiment, impact air pressures of 0.4 MPa and 0 MPa were chosen. Because the test and low-temperature compensation device equipment can stably control the temperature range, five temperature conditions, i.e., 10, − 10, − 15, − 20 and − 30 °C, were set to perform cyclic impact tests on saturated granite rock samples at different air pressures.

On the basis of one-dimensional stress wave theory, the 'three-wave method' was employed for data processing to obtain the strain rate as well as the strain and stress of the rock samples during the test. The calculation formulas are given by Eq. (1)[5–9]:

$$\begin{cases} \dot{\varepsilon}(\mathrm{t}) = \dfrac{c}{l_s}\left[\varepsilon_{\mathrm{i}}(\mathrm{t}) - \varepsilon_{\mathrm{r}}(\mathrm{t}) - \varepsilon_{\mathrm{t}}(\mathrm{t})\right] \\ \varepsilon(\mathrm{t}) = \dfrac{c}{l_s}\displaystyle\int_0^{\mathrm{t}}\left[\varepsilon_{\mathrm{i}}(\mathrm{t}) - \varepsilon_{\mathrm{r}}(\mathrm{t}) - \varepsilon_{\mathrm{t}}(\mathrm{t})\right] \\ \sigma(\mathrm{t}) = \dfrac{EA}{2A_s}\left[\varepsilon_{\mathrm{i}}(\mathrm{t}) + \varepsilon_{\mathrm{r}}(\mathrm{t}) + \varepsilon_{\mathrm{t}}(\mathrm{t})\right] \end{cases} \tag{1}$$

where $\dot{\varepsilon}(\mathrm{t})$, $\varepsilon(\mathrm{t})$, and $\sigma(\mathrm{t})$ represent the stress time ranges of the incident, reflected, and transmitted waves, respectively; A and A_s represent the cross-sections of the bar and sample, respectively; c and E represent the longitudinal wave velocity and Young's modulus of the bar, respectively; and l_s represents the height of the sample.

The stress uniformity assumption needs to be satisfied for both cyclic and single impact tests during the transmission of stress waves within a rock sample[6–11,24]. Considering examples of the stress equilibrium diagram of saturated granite during the second impact at − 10 °C and the sixth impact at − 20 °C, as shown in Fig. 3, the curve of the sum of incident and reflected waves closely aligns with that of the transmission wave in terms of trend and peak height. This indicates that the stress within the sample has reached the equilibrium state, validating the reliability of the test data.

Analysis of test results

Macroscopic destruction characteristics and number of impact cycles

The damage morphology of saturated granite at different temperatures (10, − 10, − 15, − 20, and − 30 °C) subjected to cyclic impact loading with impact air pressures of 0.2 and 0.25 MPa is shown in (Fig. 4). Although macroscopic damage in granite occurs at all temperatures, the degree of crushing is significantly different: (1) At 10 and − 10 °C, localized damage is primarily observed, with tensile cracks evident on the surface, and the shape of the crushed body is predominated by flakes and columns. (2) At − 15 °C, the rock samples appear to crack throughout, with more tensile cracks around the periphery. Additionally, the samples exhibit more columnar and flaky fragments with higher volumes. (3) At − 20 and − 30 °C, the rock samples exhibit enhanced fragmentation, with more fragments having a smaller volume. The analysis of damage characteristics revealed

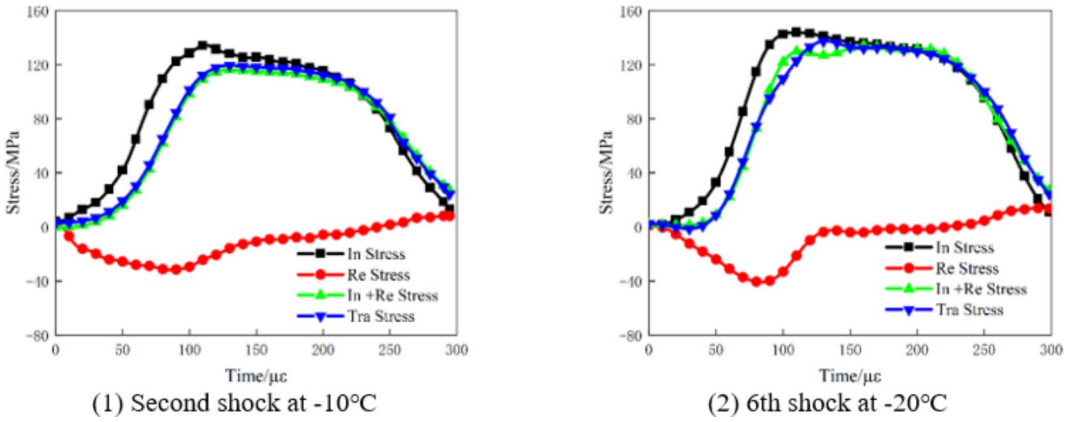

Fig. 3. Dynamic stress equilibrium diagram.

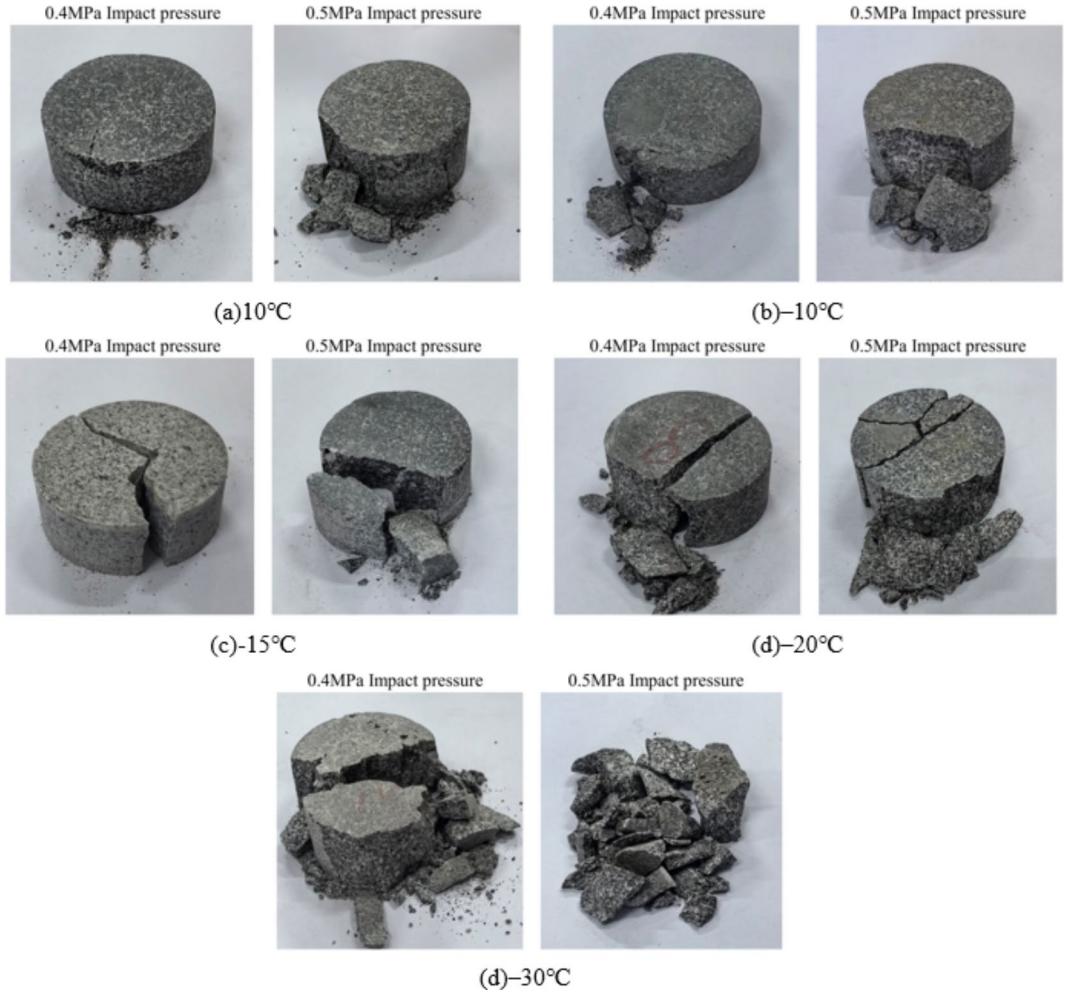

Fig. 4. Failure modes of saturated granite at different temperatures.

that the low-temperature saturated granite primarily experienced tensile damage under cyclic impact. With increasing impact air pressure, the degree of damage to the rock samples increased, and the crack extension became more obvious. At low temperatures, the rock samples as a whole are denser and show obvious freeze brittleness, which leads to an increase in the expansion of internal tension cracks when subjected to impact air pressure, with a decreasing volume and increasing number of fractures, and the damage pattern is significantly affected by the temperature change.

The relationship between the number of cyclic impacts a saturated granite sample can withstand and the temperature at both air pressures is shown in (Fig. 5). Generally, an increase in the number of cyclic impacts with decreasing temperature is observed. The saturated granite samples treated at 10 and − 10 °C can withstand a similar number of cyclic impacts, which is 4 for 0.5 MPa air pressure and approximately 10 for 0.4 MPa air pressure. The number of cyclic impacts for different impact air pressures increases significantly once the temperature reaches − 15 °C. For example, the number of cyclic impacts that can be withstood by saturated granite samples subjected to 0.5 MPa impact air pressure at − 10, − 15, − 20, and − 30 °C is 4, 4, 7, 10, and 12, respectively. At the same temperature, the number of cycles that the rock samples could withstand for 0.4 MPa air pressure is greater than that for 0.5 MPa. The analysis revealed that low-temperature conditions led to the freezing of fissure water within the saturated granite, resulting in a slight freezing expansion force that increased the densification and stability of the rock samples, thereby increasing the number of cycles. This phenomenon was further analyzed in detail in the subsequent section on changes in micromorphology. In addition, high-impact air pressure delivers greater impact energy, which accelerates the expansion of both new and existing internal cracks, exacerbates internal damage, and leads to a decrease in the number of cyclic impacts that rock samples can withstand.

Dynamic stress-strain curves

The stress-strain curves of saturated granite under cyclic impact loading at different temperatures are shown in (Figs. 6 and 7). From the general trend observed, the curves can be divided into compression-density, elasticity, microcrack expansion, and unloading stages. During the initial impacts of cyclic loading, the rock samples do not exhibit any macroscopic damage, indicating a significant level of compressive strength. The stress-strain curves remain consistent, indicating the phenomenon of post-peak rebound. This means that the strains start to decrease after reaching a certain value, indicating some resistance of the samples to deformation. In the final impact (rock macro-damage), the rebound phenomenon is not evident in the curve. This suggests that the accumulated damage in the rock samples from multiple impacts exceeded the tolerance limit, resulting in the release of some stored energy and leading to specimen failure. With an increase in the number of cyclic impacts on the rock samples, the overall trend of the dynamic stress-strain curve shifts toward the lower right. Additionally, the slope of the tangent line in the rising phase before the peak decreases, resulting in a reduction in the deformation modulus and peak stress and an increase in the peak strain.

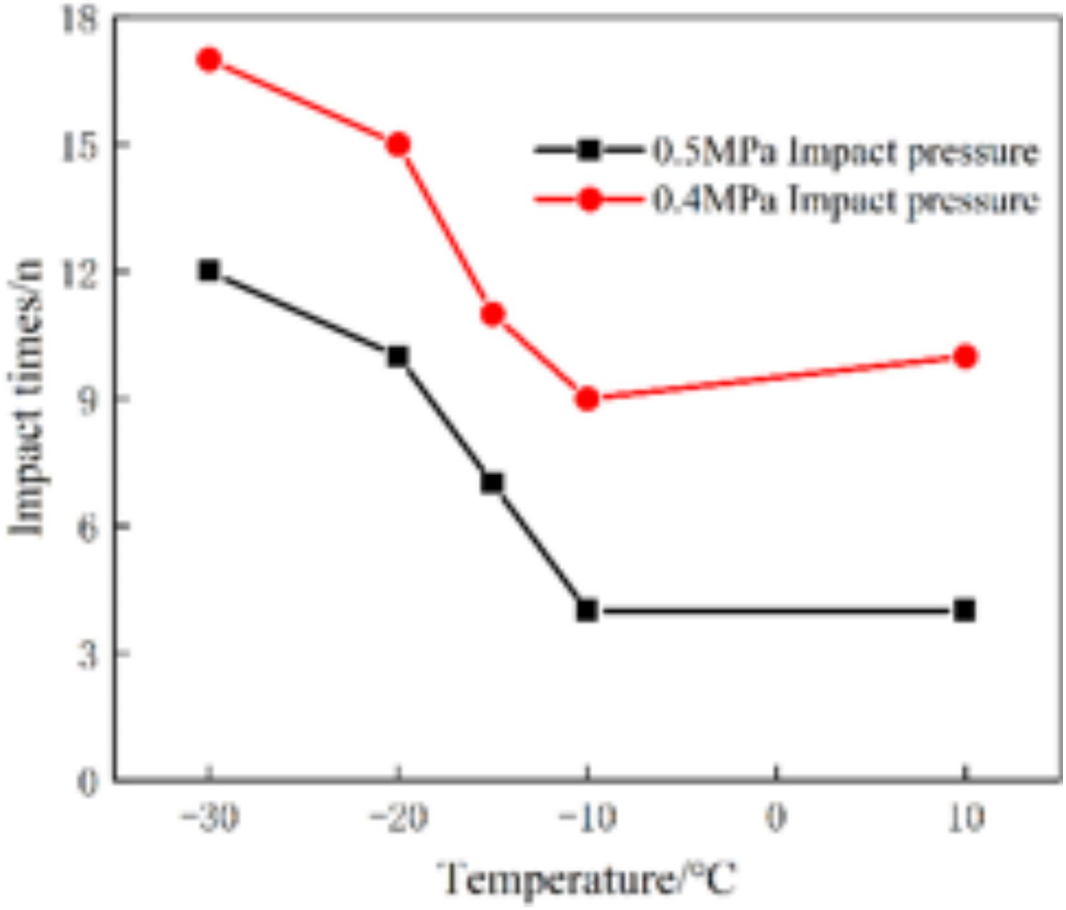

Fig. 5. Dynamic stress equilibrium diagram.

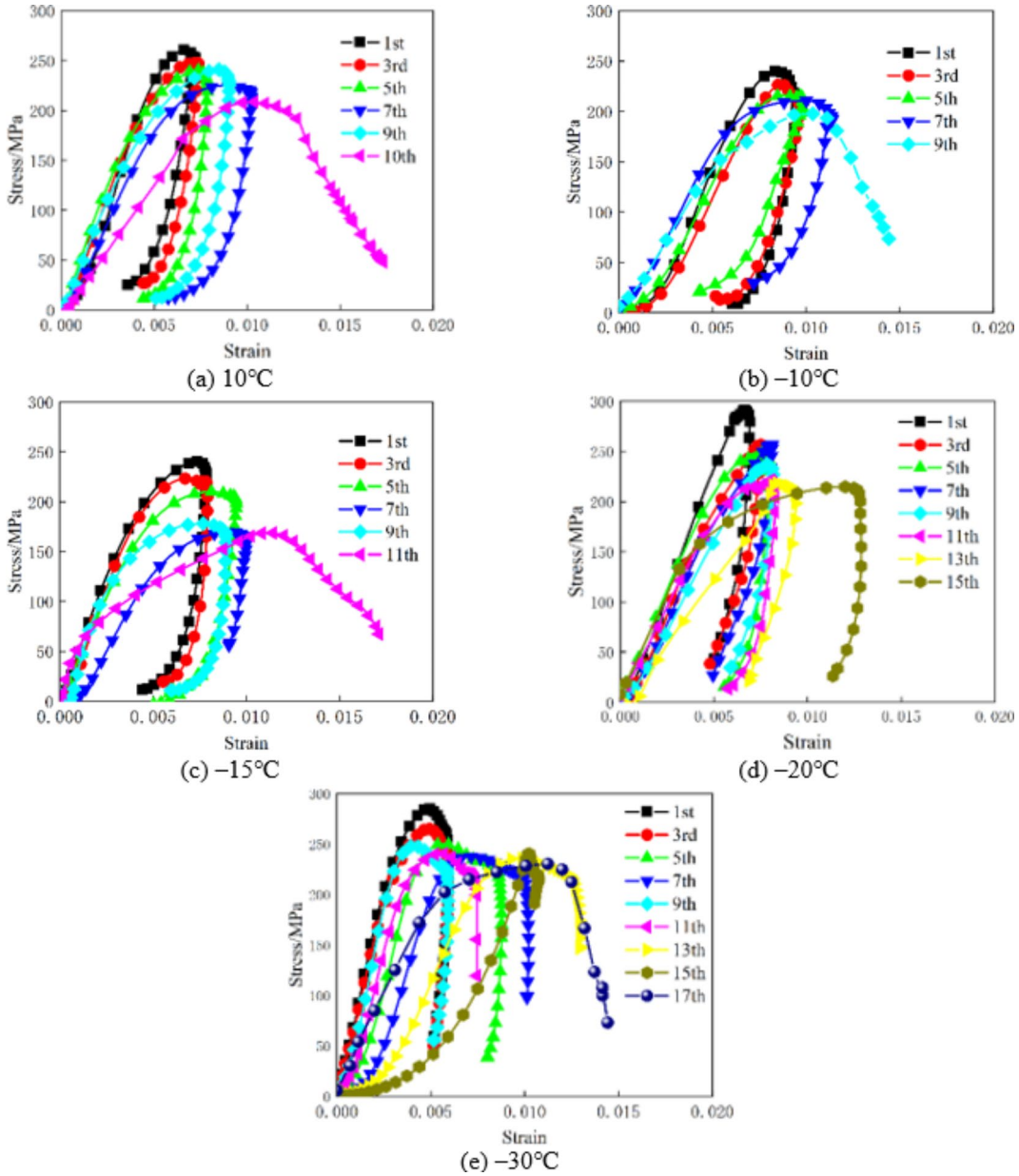

Fig. 6. Dynamic stress–strain curves of rock specimens subjected to 0.4 MPa air pressure.

Peak stress and peak strain

The variation in the peak stress with the number of impacts in granite subjected to cyclic impacts is shown in (Fig. 8). The peak stress of the rock samples at the same temperature is positively correlated with the impact air pressure, i.e., a higher impact air pressure indicates greater peak stress attained before sample destruction. For example, the initial peak stress reaches 241.93 MPa under low air pressure and 254.98 MPa under high air pressure for rock samples at −10 °C. For the saturated granite samples at −20 and −30 °C, 10 or more impact cycles are required before macroscopic damage can be observed. The peak stress slowly decreases with increasing number of impacts. A maximum decrease of 24.13% is observed for both temperatures. In contrast, for the samples heated at 10, −10 and −15 °C, no more than 10 cycles of impact are required to cause damage. Under these conditions, the peak stress decreases significantly, especially at −15 °C, where the peak stress for 0.2 MPa impact air pressure decreases by up to 34.49%. This indicates that the cycling process, when the temperature ranges from −20 to −30 °C and the saturated granite is more intact, leads to an increase in the compressive strength.

The variation in the granite peak strain with the number of impacts when subjected to cyclic loading is shown in (Fig. 9). The overall fluctuating peak strain curve of the rock samples is attributed to the variations in the elastic velocity with each impact and the instability in the amplitude of the incident wave. At the same temperature, a steeper increase in the peak strain corresponds to a higher impact air pressure. At 10 and −10 °C, the peak strain at which macroscopic failure of the rock samples occurs increases with decreasing temperature.

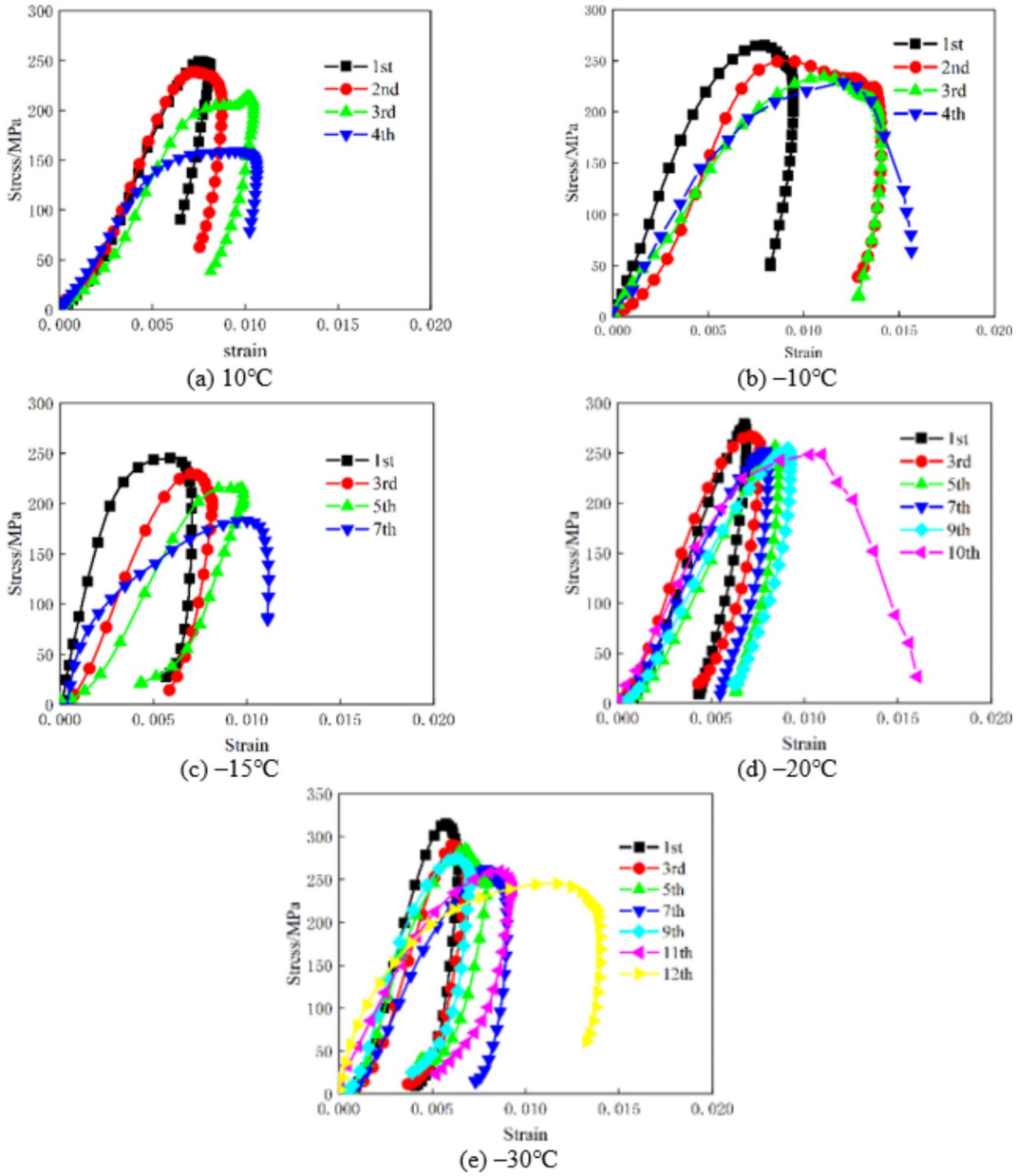

Fig. 7. Dynamic stress-strain curves of rock specimens subjected to 0.5 MPa air pressure.

This is attributed to the phase change of water to ice within the water-saturated granite, leading to freezing and expansion. This expansion exacerbates the degree of internal damage, leading to more severe fragmentation and increased peak strain under impact loading[7]. Within the range of − 15 to − 30 °C, the peak strain at which final damage occurs increases with decreasing temperature. However, it remains lower than that at 10 and − 10 °C. The increase in the peak strain of the saturated granite samples at low temperatures ranges from 22.83 to 129.23% for different impact air pressures. With an increase in the number of impacts, the internal stress concentration and damage accumulation in the rock samples become significant. When the damage threshold is reached, the strain characteristics deteriorate, and crack extension leads to macroscopic damage, whereas the number of impacts required to reach failure of rock samples at different temperatures decreases with increasing impact air pressure.

Dissipative energy analysis

After cooling, when the saturated granite samples are subjected to cyclic impact compounding, the energy absorption observed during analysis can directly reflect the degree of damage within the rock. This study is based on the effect of cyclic shock on the degradation of rock samples at different low temperatures under the same total incident energy conditions. In the cyclic shock experiment, the incident wave W_i, reflected wave W_r, and transmitted wave W_t of the rock samples are calculated as follows[25,26]:

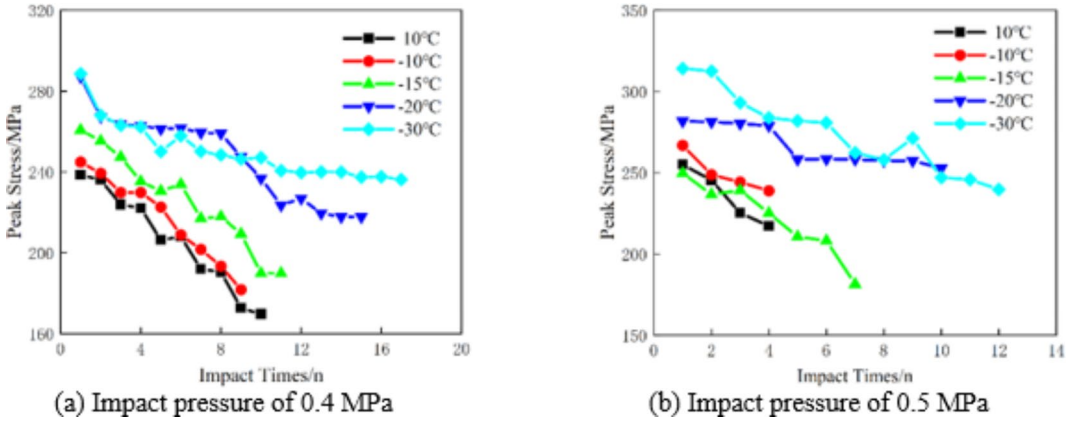

Fig. 8. Relationship between impact peak stress and cyclic impact times.

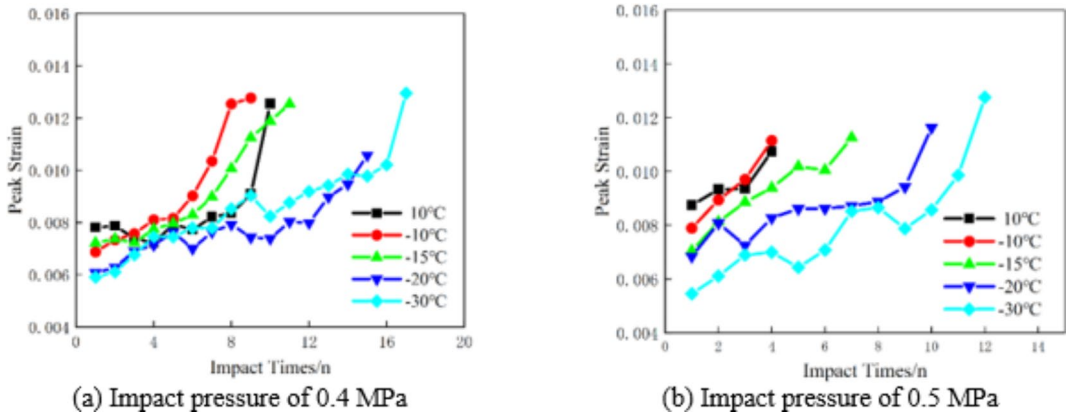

Fig. 9. Relationship between impact peak strain and cyclic impact times.

$$\begin{cases} W_{\mathrm{i}} = \left(\dfrac{Ac_0}{E_0}\right)\displaystyle\int_0^{\mathrm{t}} \varepsilon_{\mathrm{i}}^2(\mathrm{t})\mathrm{dt} \\ W_{\mathrm{r}} = \left(\dfrac{Ac_0}{E_0}\right)\displaystyle\int_0^{\mathrm{t}} \varepsilon_{\mathrm{r}}^2(\mathrm{t})\mathrm{dt} \\ W_{\mathrm{t}} = \left(\dfrac{Ac_0}{E_0}\right)\displaystyle\int_0^{\mathrm{t}} \varepsilon_{\mathrm{t}}^2(\mathrm{t})\mathrm{dt} \end{cases} \tag{2}$$

where A indicates the cross-sectional area of the rod; c_0 represents the longitudinal wave velocity; and E_0 denotes the product of the rod density ρ and ρ square.

The dissipated energy can be approximately equal to the energy absorbed by the sampleW_{s}, and this relationship can be expressed by Eq. (2). The essence of rock failure is that the degradation of rock mechanical properties and strength is attributed primarily to energy evolution, energy dissipation, and energy release[25]. To better understand the energy change dynamics of low-temperature saturated granite under cyclic impact loading, the cumulative dissipated specific energy (ϑ) was introduced, and the calculation formula can be expressed as Eq. (4)[27–29]:

$$W_{\mathrm{s}} = W_{\mathrm{i}} - W_{\mathrm{r}} - W_{\mathrm{t}} \tag{3}$$

$$E_{\mathrm{v}} = \frac{W_{\mathrm{s}}}{V_{\mathrm{s}}} \tag{4}$$

$$\vartheta = \sum_{\mathrm{i}=1}^{\mathrm{n}} E_{\mathrm{v(i)}} \tag{5}$$

where W_{s} refers to the dissipated energy of the rock sample, V_{s} represents the volume of the rock sample, E_{v} represents the dissipated energy per unit volume, ϑ represents the specific energy dissipated under the ith impact, and n represents the number of cyclic impacts.

temp	Number of shocks	Incident energy/J	Reflectance energy/J	Transmitted energy/J	temp	Number of shocks	Incident energy/J	Reflectance energy/J	Transmitted energy/J
10 °C	1	122.939	11.734	87.354	−20 °C	1	111.586	3.964	90.309
	3	128.661	11.443	94.830		3	115.641	8.455	89.261
	5	151.789	14.275	108.803		5	109.533	10.412	81.676
	7	143.749	8.567	112.697		7	104.101	3.022	85.921
	9	177.003	9.967	135.788		9	142.298	4.488	122.336
	10	161.180	11.902	119.721		11	146.814	9.434	119.716
−10 °C	1	164.213	9.578	117.349		13	124.934	4.0575	99.939
	3	177.325	10.311	138.286		15	157.126	18.491	123.325
	5	154.048	13.906	117.124	−30 °C	1	128.849	5.650	112.083
	7	130.492	15.737	95.172		3	119.391	3.236	104.138
	9	161.951	17.210	114.817		5	116.940	6.566	95.005
−15 °C	1	111.586	8.819	88.625		7	117.973	13.594	91.305
	3	110.641	9.660	85.372		9	130.122	4.122	108.986
	5	109.533	11.622	79.782		11	141.614	11.082	104.458
	7	104.101	5.901	80.072		13	122.270	10.858	101.330
	9	142.298	13.710	110.072		15	126.542	2.931	100.529
	11	109.883	4.647	86.838		17	122.323	11.236	87.390

Table 2. Incident wave, reflected wave, and transmitted wave of saturated granite at different temperatures for an impact pressure of 0.4 MPa.

temp	Number of shocks	Incident energy/J	Reflectance energy/J	Transmitted energy/J	temp	Number of shocks	Incident energy/J	Reflectance energy/J	Transmitted energy/J
10 °C	1	151.993	12.552	114.816	−20 °C	1	138.017	10.964	109.969
	2	124.702	11.142	95.411		3	140.014	10.9631	113.156
	3	132.043	11.348	100.963		5	142.097	12.738	113.302
	4	138.814	12.465	100.701		7	170.745	12.789	141.362
−10 °C	1	140.930	15.600	93.333		9	171.739	13.294	140.679
	2	132.349	18.528	85.421		11	169.043	12.812	135.448
	3	150.320	15.181	103.404	−30 °C	1	176.418	12.338	127.836
	4	112.934	18.480	65.141		3	170.617	14.724	122.067
−15 °C	1	138.017	11.353	95.354		5	159.596	12.955	125.470
	3	140.014	16.582	97.801		7	162.904	15.185	124.701
	5	142.097	14.038	103.69		9	167.130	9.191	138.356
	7	148.369	17.324	98.36		11	197.147	10.302	167.262
						12	200.763	8.573	162.266

Table 3. Incident wave, reflected wave, and transmitted wave of saturated granite at different temperatures for an impact pressure of 0.5 MPa.

The incident, reflected, and transmitted waves measured from the saturated granite samples under different test conditions, as calculated via Eq. (2), are provided in (Tables 2 and 3). These values were used to calculate the cumulative specific dissipation energy (ϑ). Figure 10 shows the relationship between the cumulative dissipation of specific energy and the number of impacts for different impact air pressures. Typically, the cumulative specific dissipation energy tends to increase with an increasing number of impacts. Before the macro-destruction of the sample, the growth rate remains relatively stable, and the specific energy of increase is less than 0.1 J cm^{-3}, with the dissipation energy increasing significantly closer to macro-destruction[27]. For an air pressure of 0.4 MPa, the cumulative specific dissipation energy of rock samples at different temperatures is 0.7527, 0.7608, 0.7408, 0.7788, and 0.8161 J cm^{-3}. Typically, the specific dissipation energy remains stable at temperatures between 10 and −15 °C. When the temperature decreases to −20 °C or below, the specific energy increases significantly and tends to be similar to that at a pressure of 0.5 MPa. At the same temperature, the growth rate of dissipative specific energy accelerates with increasing impact air pressure, especially at −20 and −30 °C, where the specific energy increases from 0.5603 and 0.7493 J cm^{-3} for pressures of 0.4 MPa to 0.7332 and 0.9426 J cm^{-3} for pressures of 0.5 MPa, respectively, at the point of final destruction. The growth trend becomes more significant with a significant increase in specific energy. Initially, it was believed that at lower ground temperatures, the moisture within the saturated granite sample freezes into ice, resulting in a freezing expansion force. To a certain extent, this force contributes to the concentration of internal stresses within the sample, leading to an increase in the

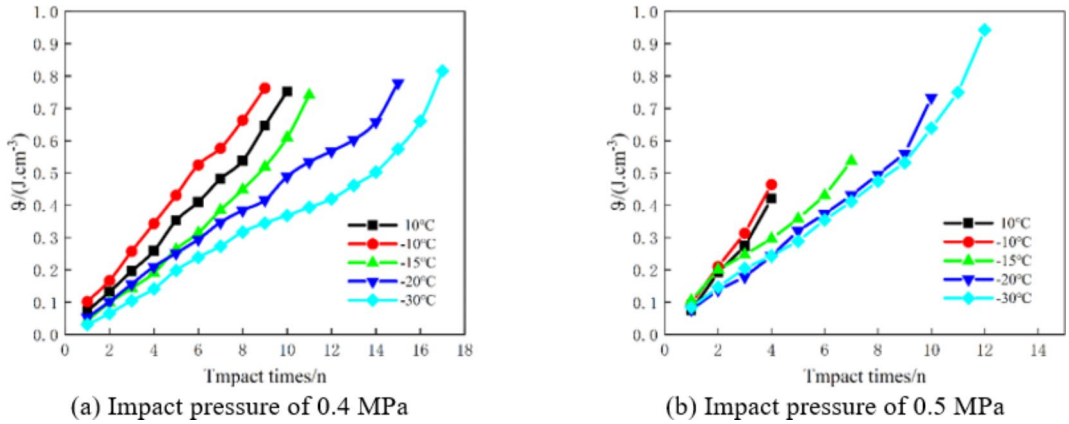

Fig. 10. Relationship between specific dissipated energy and impact times at different temperatures.

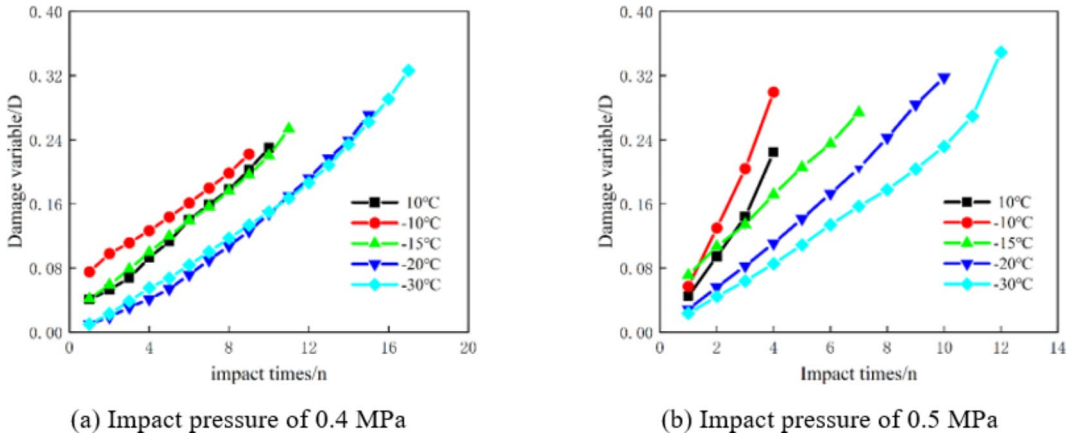

Fig. 11. Relationship between cumulative specific dissipated energy and impact times at different temperatures.

bearing capacity of the sample under impact loading. At the same time, the energy released during the ice phase transition increases the dissipated energy of the sample[17], with this increase becoming more significant as the sample approaches its damage limit.

Cumulative damage

Owing to inherent defects and nonlinear characteristics of natural rock, damage variables defined on the basis of the elastic modulus and plastic strain are more prone to overlooking anomalies[30,31]. Therefore, the cumulative damage of saturated granite at low temperatures was analyzed via the correlation between the cumulative damage factor D and the number and energy of impacts, as given by Eq. (6)[30–32]:

$$D = \frac{\sum_{i=1}^{n} W_{d,i}}{W} \tag{6}$$

where D is expressed as the ratio of $W_{d,i}$ to W, $W_{d,i}$ represents the dissipated energy of the rock under the ith cyclic impact, and W represents the total dissipated energy of the rock under cyclic impact loading.

The relationship between the cumulative damage factor and the number of impacts at different temperatures for saturated granite is shown in (Fig. 11). The cumulative damage factor gradually increases with an increasing number of cyclic impacts. The cumulative damage factor of saturated granite at lower temperatures (–20 and − 30 °C) reaches 0.2712, 0.3179 and 0.3263, 0.3491, which are higher than those at other temperatures. These findings indicate that lower temperature conditions at the surface affect the stress properties and deformation resistance of rock samples. The lower the temperature is, the greater the damage to rock samples at the same air pressure. For example, the cumulative damage factor at 0.4 MPa reaches 0.2298, 0.2221, 0.2535 and 0.2712, 0.3263, respectively, indicating that the degree of damage to saturated granite is affected by temperature. These results are consistent with the macro-damage pattern observed in (Fig. 4). As the temperature decreases, the degree of crack extension and the degree of fragmentation of the rock samples increase significantly. This

phenomenon is consistent with the trend of the cumulative damage factor; specifically, as the temperature decreases, the rock samples are subjected to more impact air pressure, the damage factor gradually accumulates, and the energy required to promote crack propagation increases. When the damage factor reaches the damage threshold of a rock sample, the sample will crack or spall, resulting in other fracture phenomena, and the larger the cumulative damage value is, the more severe the degree of damage. Moreover, as the impact air pressure increases, the cumulative damage factor also increases (i.e., the slope of the curve becomes steeper). The rate of damage development in saturated granite is positively correlated with the impact velocity. Briefly, low-temperature saturated granite continuously exchanges energy with its surrounding environment during the cyclic impact process and undergoes a damage evolution process by energy depletion. The relationship between the cumulative damage factor and the peak dynamic stress is shown in (Fig. 12). Overall, with increasing cumulative damage factor, the peak dynamic stress of the saturated granite at all temperatures tends to decrease, indicating a negative correlation between the two parameters.

SEM analysis

The cross-sectional structure of the low-temperature saturated granite samples subjected to cyclic impact loading was analyzed by scanning electron microscopy (SEM). Figure 13 shows SEM images of the cross-sections of saturated granite rock samples subjected to cyclic impact loading at different temperatures. As shown in Fig. 12, the cross-sectional morphology of the rock samples varies with temperature, primarily exhibiting a river-type pattern formed by crystal disintegration, a step-type pattern, a stripe-type pattern due to crystal slip[33], and a secondary fracture pattern resulting from multiple impacts and successive damage. The cross-sectional morphology of saturated granite under cyclic impact loading at 10 °C is slightly rougher, with a small fraction of stripe-type patterns, as well as less pronounced river-type and step-type patterns, with fewer secondary fracture lines. As the temperature decreased to −10 and − 15 °C, the flatness of the cyclic action-saturated granite fractures decreased, and the proportions of step and river fracture patterns increased significantly. At lower temperatures, the coverage of brittle fracture cracks expanded and increased in number, and slip separation occurred in some areas. When the temperature was further lowered to − 20 and − 30 °C, the rock samples presented more obvious freeze brittleness characteristics at the macroscopic level. Scanning electron microscopy (SEM) images revealed that the brittle fracture cracks almost completely covered the damaged surface, the flatness of the section was greatly reduced, the proportion of step-type fracture morphology significantly increased, and the slip separation phenomenon became more obvious. These results indicate that the granite samples subjected to low-temperature saturation exhibit more pronounced freeze brittleness at lower temperatures and that the degree of fragmentation significantly increases.

Combined with the trends of the cumulative damage factor shown in (Fig. 10a,b), the cumulative damage factor gradually increases with increasing temperature. This change results in increasing energy accumulation in rock samples, which promotes the macroscopic expansion of cracks. At the microscopic level, the fracture flatness of rock samples gradually decreases, the area of brittle fracture cracks gradually expands to cover the entire damaged surface, the phenomenon of slip separation becomes increasingly obvious, and these phenomena are positively correlated with the change in the cumulative damage value. Therefore, the deformation and damage process of rock samples fully reflects the damage evolution characteristics of energy dissipation.

Conclusion

(1) The macro-damage of low-temperature saturated granite is attributed primarily to tensile damage. Under the same air pressure conditions, the number of cyclic impacts required to reach macroscopic damage remained stable until the temperature decreased to 15 °C and then tended to increase. The rock samples were generally denser at low temperatures and exhibited freeze brittleness; the expansion of internal tensile

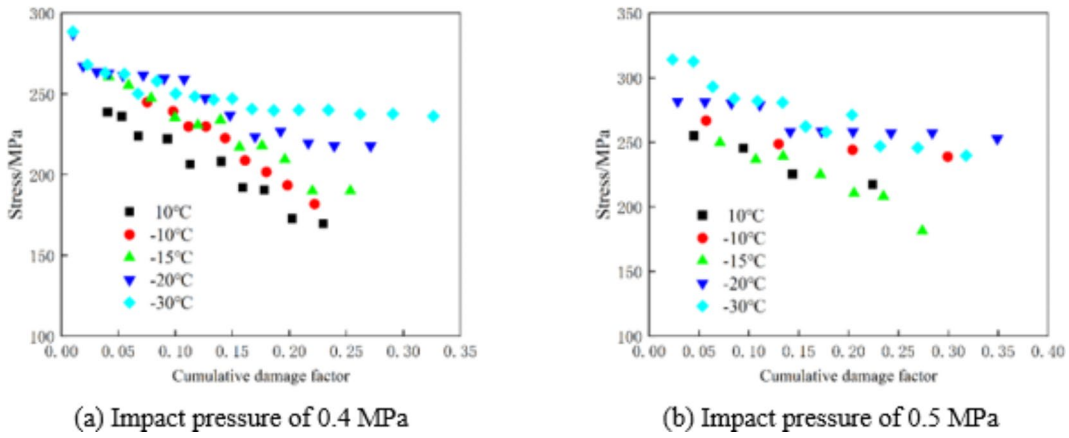

Fig. 12. Relationship between cumulative specific dissipated energy and dynamic stress at different temperatures.

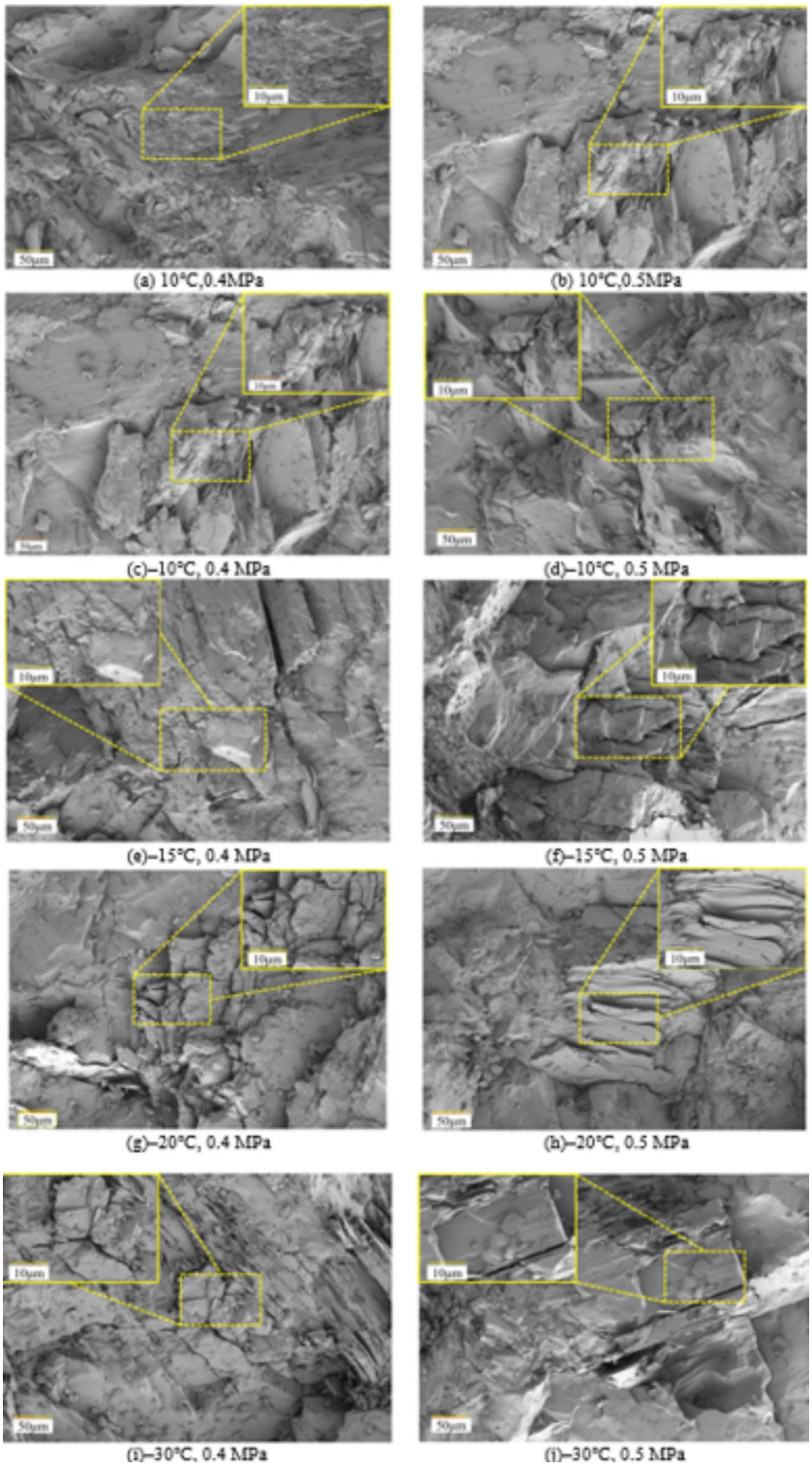

Fig. 13. Microstructure of saturated granite subjected to cyclic impact loading at different temperatures.

cracks increased under impact, the volume of fragmentation decreased, the number of cracks increased, and the damage pattern was significantly affected by temperature.

(2) The dynamic stress-strain curves in the tests generally exhibited rebound characteristics after the peak stress, and the curves shifted to the lower right overall. With the increase in the number of cyclic shocks, the peak stress of the rock samples at each temperature shows an overall decreasing trend, whereas the peak strain and cumulative dissipation-specific energy change in the opposite trend, especially in the lower-temperature environment. The trend of peak stress reduction is more evident, and the peak strain and cumu-

lative dissipation specific energy increase as the amplitude increases, and those near the macro-damage increase faster.

(3) There was a gradual increase in the aggregated damage factor of the rock samples subjected to cyclic impact loading, with the aggregated damage factor being greater at low temperatures than at other temperatures, which was consistent with the degree of crack extension and fracture of the macroscopic rock samples. Moreover, the peak dynamic stress of saturated granite at each temperature was negatively correlated with the increase in the aggregated damage factor. This demonstrated that the combined influence of low-temperature loading and cyclic impact loading led to varying degrees of influence on the degradation of the mechanical properties and deformation resistance of saturated granite.

(4) SEM analysis of the fracture morphology of low-temperature saturated granite after cyclic impact reveals that impact loading significantly affects the morphology of low-temperature rock. With decreasing temperature, the fracture exhibited more pronounced freeze brittleness, the area of brittle fracture cracks gradually extended to the entire damage surface, the slip separation phenomenon became more obvious, and these phenomena were positively correlated with the change in the cumulative damage value.

Data availability

Data is provided within the manuscript.

Received: 11 July 2024; Accepted: 23 September 2024
Published online: 05 November 2024

References

1. Luo, Y., Gong, F., Li, X. & Wang, S. Experimental simulation investigation of influence of depth on spalling characteristics in circular hard rock tunnel. *J. Cent. South. Univ.* **27**, 891–910. https://doi.org/10.1007/s11771-020-4339-5 (2020).
2. Cerfontaine, B. & Collin, F. Cyclic and fatigue behaviour of rock materials: review, interpretation and research perspectives. *Rock. Mech. Rock. Eng.* **51**, 391–414. https://doi.org/10.1007/s00603-017-1337-5 (2018).
3. Yang, J., Wu, Z., Sun, W., Yao, C. & Wang, Q. Numerical simulation on radiation and energy of blast-induced seismic waves in deep rock masses. *J. Cent. South. Univ.* **29**, 645–662. https://doi.org/10.1007/s11771-022-4908-x (2022).
4. Wang, S., Huang, L. & Li, X. Analysis of rockburst triggered by hard rock fragmentation using a conical pick under high uniaxial stress. *Tunn. Undergr. Sp Tech.* **96**, 103195. https://doi.org/10.1016/j.tust.2019.103195 (2020).
5. Jin, J. F., Li, X. B., Chang, J. R., Tao, W. & Qiu, C. Stress-strain curve and stress wave characteristics of rock subjected to cyclic impact loadings. *Explo Shock Waves* **33**, 613–619. https://doi.org/10.11883/1001-1455(2013)06-0613-07 (2013).
6. Li, X., Lok, T. & Zhao, J. Dynamic characteristics of granite subjected to intermediate loading rate, Rock Mech. *Rock. Eng.* **38**, 21–39. https://doi.org/10.1007/s00603-004-0030-7 (2005).
7. Wang, Z. L., Yang, H. & Tian, N. C. Mechanical property and damage evolution mechanism of granite under uniaxial cyclic impact. *J. Harbin Inst. Tech.* **52**, 59–66. https://doi.org/10.11918/201811085 (2020).
8. Shu, R. H. et al. Effect of thermal treatment on energy dissipation of granite under cyclic impact loading. *J. Trans. Nonferrous Met. Soc. Ch.* **29**, 385–396. https://doi.org/10.1016/S1003-6326(19)64948-4 (2019).
9. Ping, Q., Ma, Q. Y., Lu, X. Y. & Yuan, W. Impact compression test of rock material under passive confining pressure conditions. *Chin. J. Vib. Shock* **33**, 55–59. https://doi.org/10.3969/j.issn.1000-3835.2014.02.011 (2014).
10. Cao, R. et al. Damage characteristics and fracture behaviour of marble after cycle impact loading. *Theor. Appl. Fract. Mec.* **125**, 103903. https://doi.org/10.1016/j.tafmec.2023.103903 (2023).
11. Yavuz, H. et al. Estimating the index properties of deteriorated carbonate rocks due to freeze thaw and thermal shock weathering. *J. Int. J. Rock. Mech. Min. Sci.* **43**, 767–775. https://doi.org/10.1016/j.ijrmms.2005.12.004 (2006).
12. Yang, G. S. et al. Research progress and tendency in characteristics of multiscale damage mechanics of rock under freezing-thawing. *J. Chin. J. Rock. Mech. Eng.* **37**, 545–775. https://doi.org/10.13722/j.cnki.jrme.2017.1295 (2018).
13. Zhang, H. M., Meng, X. Z. & Peng, C. Rock damage constitutive model based on residual intensity characteristics under freeze-thaw and load. *J. J. Ch. Coal Soc.* **44**, 3404–3411. https://doi.org/10.13225/j.cnki.jccs.2018.1681 (2019).
14. Liu, S. et al. An experimental study on the physico-mechanical properties of two post-high-temperature rocks. *J. Eng. Geol.* **71**, 188–193. https://doi.org/10.1016/j.ijrmms.2014.07.008 (2014).
15. Liu, S. & Xu, J. Y. Estimating the index properties of deteriorated carbonate rocks due to freeze thaw and thermal shock weathering. *J. Int. J. Rock. Mech. Min. Sci.* **185**, 63–70. https://doi.org/10.1016/j.enggeo.2014.11.013 (2015).
16. Yin, T. B. et al. Effect of thermal treatment on the mode I fracture toughness of granite under dynamic and static coupling lead. *J. Eng. Fract. Mech.* **199**, 143–158. https://doi.org/10.1016/j.engfracmech.2018.05.035 (2018).
17. Huang, Z., Wei, J., Li, G. & Cai, C. An experimental study of tensile and compressive strength of rocks under cryogenic nitrogen freezing. *Rock. Soil. Mech.* **37**, 694–700 (2016).
18. Wang, J. et al. Low temperature effect of dynamic characteristics of water-saturated granite at high strain rate. *Rock. Soil. Mech.* **38**, 163–169 (2017).
19. Zhang, R. R., Shen, Y. H., Ma, D. D., Ping, Q. & Yang Study on dynamic characteristics and damage mechanism of freeze-thaw treated red sandstone under cyclic impact. *J/OL Explos. Shock Waves* **38**, 163–169. https://doi.org/10.11883/bzycj-2023-0449 (2024).
20. Meng, X. Z. et al. Damage constitutive prediction model for rock under freeze–thaw cycles based on mesoscopic damage definition. *J. Eng. Fract. Mech.* **293**, 109–685. https://doi.org/10.1016/j.engfracmech.2023.109685 (2023).
21. Shu, R., Yin, T., Li, X., Yin, Z. & Tang, L. Effect of thermal treatment on energy dissipation of granite under cyclic impact loading. *T Nonferr. Metal Soc.* **29**, 385–396. https://doi.org/10.1016/S1003-6326(19)64948-4 (2019).
22. Wang, Z., Tian, N., Wang, J., Liu, J. & Hong, L. Experimental study on damage mechanical characteristics of heat-treated granite under repeated impact. *J. Mater. Civil Eng.* **30**, 04018274. https://doi.org/10.1061/(ASCE)MT.1943-5533.0002465 (2018).
23. Wang, Z., Tian, N., Wang, J., Yang, S. & Liu, G. Mechanical response and energy dissipation analysis of heat-treated granite under repeated impact loading. *Comput. Mater. Con.* **59**, 275–296. https://doi.org/10.32604/cmc.2019.04247 (2019).
24. Song, L. & Hu, S. Two-wave and three-wave method in SHPB data processing, Explo. *Shock Waves* **25**, 368 (2005).
25. Lundberg, B. A split Hopkinson Bar study of energy absorption in dynamic rock fragmentation. *Int. J. Rock. Mech. Min. Sci. Geomech. Abstracts* **13**, 187–197. https://doi.org/10.1016/0148-9062(76)91285-7 (1976).
26. Xia, K. & Yao, W. Dynamic rock tests using split Hopkinson (Kolsky) bar system–A review. *J. Rock. Mech. Geotech.* **7**, 27–59. https://doi.org/10.1016/j.jrmge.2014.07.008 (2015).
27. Wang, Z. L., Wang, D. W. & Wang, S. M. Dynamic behaviors and energy dissipation characteristics of marble under cyclic impact loading explosion and shock waves. *Explo Shock Waves* **33**, 613–619. https://doi.org/10.11883/1001-1455(2013)06-0613-07 (2013).

28. Peng, K., Liu, Z., Zou, Q., Wu, Q. & Zhou, J. Mechanical property of granite from different buried depths under uniaxial compression and dynamic impact: an energy-based investigation. *Powder Technol.* **362**, 729–744. https://doi.org/10.1016/j.powtec.2019.11.101 (2020).
29. Ran, Q. C. et al. Experimental investigation on mechanical characteristics of red sandstone under graded cyclic loading and its inspirations for stability of overlying strata. *Geomech. Geophys. Geo.* **9**, 11. https://doi.org/10.1007/S40948-023-00555-X (2023).
30. Liu, Y., Dai, F., Dong, L., Xu, N. & Feng, P. Experimental investigation on the fatigue mechanical properties of intermittently jointed rock models under cyclic uniaxial compression with different loading parameters, Rock Mech. *Rock. Eng.* **51**, 47–68. https://doi.org/10.1016/j.ijrmms.2018.04.041 (2018).
31. Zhao, G., Xie, L. & Meng, X. A damage-based constitutive model for rock under impacting load. *Int. J. Min. Sci. Technol.* **24**, 505–511. https://doi.org/10.1016/j.ijmst.2014.05.014 (2014).
32. Li, M. et al. Effect of specimen size on energy dissipation characteristics of red sandstone under high strain rate. *Int. J. Min. Sci. Technol.* **24**, 151–156. https://doi.org/10.1016/j.ijmst.2014.01.002 (2014).
33. Dong, B. *Experimental Study on the Dynamic Properties and Energy Consumption char-acteristics of Granite under Cyclic Impact Loading* (Henan Polytechnic University, 2022).

Acknowledgements

This work was supported by the National Major Research Instrument Development Program (No. 52227901).

Author contributions

Conceptualization, H.X. and C.R.; methodology, H.X. and B.W.; data curation, H.X., C.R. and B.W.; writing—original draf, H.X.; writing—review and editing, H.X. and B.W.; visuali-zation, C.R. and Q.Z.; supervision, Z.S. and Y.J. All authors have read and agreed to the pub-lished version of the manuscript.

Declarations

Competing interests

The authors declare no competing interests.

Additional information

Correspondence and requests for materials should be addressed to C.R.

Reprints and permissions information is available at www.nature.com/reprints.

Publisher's note Springer Nature remains neutral with regard to jurisdictional claims in published maps and institutional affiliations.